height field averaged over the three forecasts obtained from our technique at lead times of 6 to 8 months is good (Fig. 1) in selected regions of the globe, particularly the tropical oceans and land masses and the northern Pacific Ocean (Aleutian Low). The forecast is moderately good in the mid-latitude of the Southern Hemisphere and over much of North America and central Eurasia. The forecasts are quite poor over Europe, eastern North America, and Southeast Asia. However, in balance, the forecast with a 6-month lead time captured many of the major atmospheric anomalies of the remarkable winter of 1982 to 1983.

The largest cold ENSO event observed in the last 20 years occurred in the winter of 1988 to 1989. The forecast for this winter (Fig. 2) successfully captured the weakening of the Aleutian Low, the intensification of the ridge over the United States and the Atlantic, and the deepening of the Icelandic Low. As with the forecast for the warm ENSO event, this forecast is poor over Europe and much of Asia. The tropics are only moderately well depicted; the largest failing is in the central equatorial Pacific where the observations show a weak negative anomaly (an association one would not expect on the basis of numerous empirical studies).

Are these forecast results fortuitous or genuine? A detailed statistical evaluation of the forecasts by a Monte Carlo technique shows that the skill of the model in much of the tropics and central North Pacific has significance levels of 0.05 or better, whereas the skill of the model in regions of moderately good forecasts noted above has significance levels of 0.10. Another type of evaluation is to compute the simultaneous wintertime relation between tropical SST and 700-mbar height (*10*). The results (Fig. 3) show that the best relation between the variables is associated with warm or cold SST anomalies in the central equatorial Pacific and lower or higher than normal heights in the central Pacific, eastern Asia, and the subtropical Atlantic, whereas pressure in most of North America and southern Asia was higher or lower than normal. A comparison of Figs. 1 and 3 shows that the forecast is good in just the regions that one would expect from the empirical studies. Reversing the signs of the anomalies on Fig. 3, to represent a cold event situation, gives the same conclusions. Data for the Southern Hemisphere are not adequate to establish a similar empirical comparison.

The above result raises a final question: Why not use a statistical model in place of the AGCM and the forecast SST in a much simpler two-tiered forecast scheme? There are two clear answers to this question. (i) In many parts of the world the data are not adequate to construct such statistical models. Thus, the scheme presented here, or something like it, is the only hope for long-range climate forecasts in these data-sparse regions. (ii) Complex, highly nonlinear climate variables such as precipitation are not very amenable to statistical forecasting. This is illustrated in Fig. 4 where the correlation between forecast precipitation by our approach and observation is compared with the correlation between simultaneously observed winter SST and precipitation, the latter being a nowcast. This is clearly an unfair test for our forecast scheme. But the nowcast is only slightly better than the forecast with a two-season lead time in the southwestern United States. The forecast is slightly better in the southeastern region. Most important, the forecast has skill over the eastern third of the nation whereas the nowcast has none. We conclude that our approach carries skill not likely to be found in a purely statistical competitor.

The forecast skills described above suggest that our approach can provide highly useful predictions of climatic anomalies associated with ENSO events during the northern winter for lead times of at least 6 months. The success of the method relies on the prediction and occurrence of a significant warm or cold event. Such events occur every 2 to 4 years, so we do not expect our method to give reliable predictions every year. But the largest events tend to have the largest societal impact, and those appear amenable to our approach.

REFERENCES AND NOTES

1. T. P. Barnett, *Mon. Weather Rev.* **109**, 1021 (1981); A. Broccoli and R. Harnack, *ibid.*, p. 2107; T. P. Barnett and R. W. Preisendorfer, *J. Atmos. Sci.* **35**, 1771 (1978); *Mon. Weather Rev.* **115**, 1825 (1987); R. Harnack, J. Harnack, J. Lanzante, *ibid.* **114**, 1950 (1986).
2. T. P. Barnett, *J. Phys. Oceanogr.* **11**, 1043 (1981).
3. J. Shukla and J. M. Wallace, *J. Atmos. Sci.* **40**, 1613 (1983); M. Latif, J. Biercamp, H. von Storch, M. J. McPhaden, E. Kirk, *J. Clim.* **3**, 509 (1990); N. C. Lau and M. Nath, *ibid.*, p. 965; K. Arpe, L. Bengtsson, E. Roeckner, in preparation.
4. T. P. Barnett, E. Kirk, M. Latif, E. Roeckner, *J. Clim.* **4**, 487 (1991).
5. D. Neelin *et al.*, *Clim. Dyn.* **7**, 73 (1992); K. Miyakoda, A. Rosati, R. Gudgel, *Global Climate Change* (*NATO Advanced Study Institute Series*, Springer-Verlag, Berlin, 1993); K. Miyakoda, J. Sirutis, A. Rosati, R. Gudgel, in *Proceedings of the Workshop on Japanese-Coupled Ocean Atmosphere Response Experiments* (Meteorology Research Report, Geophysics Institute, University of Tokyo, Tokyo, 1989), p. 93; K. Miyakoda, J. Sirutis, A. Rosati, J. Derber, in *Proceedings of U.S.–PRC International Tropical Oceans and Global Atmosphere Project (TOGA) Symposium*, C. Jiping and J. Young, Eds. (China Ocean Press, Beijing, 1988), p. 417.
6. M. A. Cane and S. E. Zebiak, *Science* **228**, 1085 (1985); N. E. Graham, J. Michaelsen, T. P. Barnett, *J. Geophys. Res.* **92**, 14271 (1987); S. Zebiak and M. Cane, *Mon. Weather Rev.* **115**, 2262 (1987); T. Barnett *et al.*, *Science* **241**, 192 (1988).
7. T. P. Barnett, N. Graham, M. Latif, S. Pazan, W. White, *J. Clim.*, in press.
8. M. Latif, *J. Phys. Oceanogr.* **17**, 246 (1987).
9. E. Roeckner *et al.*, *Max-Planck-Inst. Meteorol. Rep. No. 93* (October 1992).
10. N. E. Graham, *Clim. Dyn.*, in press; patterns shown in Fig. 3 are for 19 years of observations, 1970 to 1989.
11. This work was supported by National Science Foundation grant ATM88-14571 and National Oceanic and Atmospheric Administration grant NA26GP0078-01 under the TOGA Program of Prediction.

6 April 1993; accepted 8 June 1993

A Solid Sulfur Cathode for Aqueous Batteries

Dharmasena Peramunage and Stuart Licht*

Because of its high resistivity and subsequent low electroactivity, sulfur is not normally considered a room-temperature battery cathode. An elemental sulfur cathode has been made with a measured capacity of over 900 ampere·hours per kilogram, more than 90 percent of the theoretical storage capacity of solid sulfur at room temperature, accessed by means of a lightweight, highly conductive, aqueous polysulfide interface through the electrocatalyzed reaction $S + H_2O + 2e^- \rightarrow HS^- + OH^-$. This solid sulfur cathode was first used in a battery with an aluminum anode for an overall discharge reaction $2Al + 3S + 3OH^- + 3H_2O \rightarrow 2Al(OH)_3 + 3HS^-$, giving a cell potential of 1.3 volts. The theoretical specific energy of the aluminum-sulfur battery (based on potassium salts) is 910 watt·hours per kilogram with an experimental specific energy of up to 220 watt·hours per kilogram.

There is a critical need for new electrochemical storage concepts that address future societal needs for consumer batteries and the propulsion of electric vehicles (*1*, *2*). The search for contemporary batteries has blurred the conventional distinctions of electrochemical storage systems. For example, candidates for electrochemical propulsion include mechanically rechargeable primary batteries, secondary batteries, and fuel cells (*2*). There has been considerable interest in nonaqueous electrolytes (such as chloroaluminate), ambient-temperature molten

---

Department of Chemistry, Clark University, Worcester, MA 01610.
*To whom correspondence should be addressed.

salt electrolytes (*3*), and a variety of lithium batteries. However, when compared to aqueous systems, these have certain environmental and cost disadvantages; consequently, aqueous batteries continue to dominate both the consumer and electric vehicle market (*1*). There have been few high-capacity aqueous cathodes introduced in the last half century, with the exception of the metal hydrides (*4*) and oxygen or air cathodes, for which many challenges remain (*5*). Of the older aqueous cathodes, lead oxide, manganese dioxide (theoretical capacity, 280 A·hour/kg), and nickel hydroxide predominate (*6*).

The low weight and cost of sulfur make it an attractive candidate for electrochemical energy storage. Molten sulfur systems, such as the sodium sulfur battery, are operated at temperatures of 300° to 350°C, maintaining the components in a liquid state for adequate electrolyte conductivity. However, material and safety constraints associated with high temperatures, corrosion, thermal cycling, and cell fabrication have slowed their development (*2, 6*).

At low (room) temperatures, elemental sulfur is a highly insoluble, insulating solid and is not expected to be a useful cathode material. Sulfur will, however, dissolve in aqueous sulfide solutions, which may be used, for example, in a reversible, low-concentration aqueous polysulfide (cathode)–tin (anode) battery (*7*). In 1987, we (*8*) presented an aqueous cathode based on highly concentrated polysulfide solution reduction

$$S_4^{2-} + 4H_2O + 6e^- \rightarrow 4HS^- + 4OH^- \qquad (1)$$

where $E°$ = −0.51 V versus a standard hydrogen electrode (SHE). The high capacity of this cathode is a result of the anomalously high solubility of potassium polysulfide salts. In excess of 25 molal (*m*) reducible sulfur can be added to saturated aqueous K_2S at room temperature (*8*). The resultant electrolyte can contain more total sulfur than water, yet operates at room temperature and is highly conductive. In accordance with Eq. 1, at 25°C, the solubility of K_2S_4 is consistent with a maximum charge capacity of 500 A·hour per kilogram of solution. This led to the introduction of an aluminum-sulfur aqueous battery with a specific energy of up to 170 W·hour/kg (*9*).

We report a cathode capable of the direct reduction of elemental sulfur at room temperature (Fig. 1). The maximum storage capacity is substantially increased and is given by the limit as all solid sulfur is reduced

$$S + H_2O + 2e^- \rightarrow HS^- + OH^- \qquad (2)$$

for which $E°$ = −0.51 V versus SHE. The theoretical storage capacity of the solid sulfur cathode [1070 A·hour/kg (*10*)] is several times larger than that of conventional aqueous cathodes, including PbO_2, NiOOH, MnO_2, HgO, and AgO (*6*).

The cathode features solid sulfur in contact with a polysulfide solution saturated in sulfur (Fig. 1A). Initiation of reductive discharge of the cell will generate polysulfide species with shorter chain lengths (Fig. 1B)

$$3S_4^{2-} + 2e- \rightarrow 4S_3^{2-} \qquad (3)$$

Further reactions proceed with dissolution and continued reduction of available solution and solid-phase sulfur

$$S_3^{2-} + S \rightarrow S_4^{2-} \qquad (4)$$

Discharge continues until all available zero-valent sulfur (both solid and dissolved) is reduced in accordance with Eq. 1. The solid sulfur maintains longer chain polysulfide species in solution, which positively shift and maximize the cell voltage (*8*). This elemental (solid-solution phase) sulfur cathode has the theoretical advantage of higher storage capacity and higher cell voltage.

Direct evidence supporting the proposed mechanism of solid sulfur cathode discharge (Eqs. 2 to 4) is found in the solubility limit [three (zero-valent) sulfurs per dissolved K_2S in saturated polysulfide solutions (*8*)] and the measured discharge of sulfur cathodes. The solid sulfur cathode exhibits an experimental discharge capacity in excess of 900 A·hour/kg (Fig. 2), an increase of 80% over that of the polysulfide cathode (*9*). To ensure that the majority of the coulombic capacity resides in the solid sulfur rather than the polysulfide, one uses an aqueous K_2S_2 rather than an aqueous K_2S_4 interface. The experimental cathode (Fig. 2, circles) consists of 50% sulfur and 50% disulfide solution interface by mass. The cathode contained a theoretical capacity of 836 A·hour/kg attributable to solid sulfur and 81 A·hour/kg attributable to the interfacial aqueous disulfide (containing two electrons per molecule of K_2S_2). The experimental discharge capacity of 903 A·hour/kg includes the mass of the polysulfide interface but not the additional mass contributions of the electrical contacts, the cell container, or the electrocatalytic current collector [the latter has a mass of 0.038 g/cm^2 for a thin film of CoS deposited on a 25-μm brass electrode (*9*), equivalent to 33 g of electrode per kilogram of solid sulfur cathode]. The addition of 4.9 *m* KOH to the disulfide interface can diminish the cathodic potential (Fig. 2, inset) but also compensates for

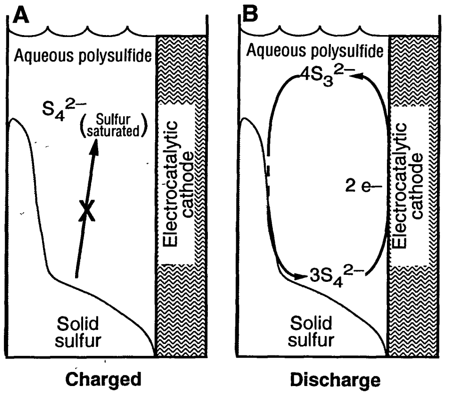

Fig. 1. Schematic representation of the solid sulfur cathode in its (**A**) charged state and (**B**) discharging state.

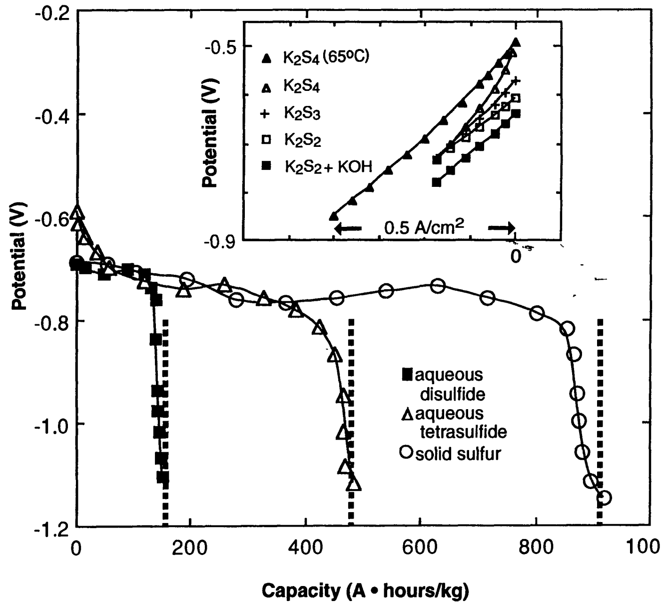

Fig. 2. Comparison of the storage capacity of the solid sulfur or polysulfide cathodes (*26*). Potentials measured versus SHE. Cathodes galvanostatically discharged at 60 mA and 35°C, each weighing 3.45 g: aqueous disulfide (squares), 2.28 ml of 6.5 *m* K_2S_2 and 4.9 *m* KOH; aqueous tetrasulfide (triangles), 2.25 ml of 7.7 *m* K_2S_4; solid sulfur (circles), 1.72 g sulfur and 1.73 g (1.14 ml) of 6.5 *m* K_2S_2 and 4.9 *m* KOH. The dashed lines refer to the theoretical charge capacities of the respective cathodes. (**Inset**) Discharge polarization of several aqueous concentrated polysulfide electrolytes at a thin-film CoS electrode and at 50°C or as indicated.

the highly alkaline anolytes that were used in the separated anode half-cell during these discharge tests. Each of the polysulfide or sulfur-polysulfide cathodes may be reduced at faradaic efficiencies approaching 100% (Fig. 2, dashed lines); thin films of CoS provide effective electrocatalysts for polysulfide reduction (*11*).

Further evidence for the dominant role of trisulfide and tetrasulfide species in Eqs. 3 and 4 is found in the electrochemistry of tetrasulfide (*12, 13*), in the enhanced rate of sulfur dissolution in solutions containing high rather than low ratios of (dissolved) sulfur to sulfide (*14, 15*), and in the near ultraviolet–visible absorption spectroscopy of aqueous polysulfide solutions. Aqueous solutions containing sulfur and a sulfide salt, M_xS_y, result in extensive speciation and a complex equilibrium of $M^{(2y/x)+}$, H_2S, HS^-, S^{2-}, S_2^{2-}, S_2^-, S_3^{2-}, S_4^{2-}, S_5^{2-}, H_2O, H^+, and OH^-. The associated equilibria have been investigated and described (*16–21*). Spectroscopic evidence shows that upon sulfur dissolution or pH modification, several distinguishable absorption peaks appear, in particular, a disulfide peak at 354 nm that diminishes with the formation and growth of a 302-nm trisulfide peak. Further sulfur addition diminishes the trisulfide peak with the formation of a 372-nm tetrasulfide peak and a 296-nm pentasulfide peak (*20*). The variation of polysulfide species during cathode discharge can therefore be determined (Table 1). During the majority of the discharge, solid sulfur is in contact with the polysulfide interface, the cell becomes saturated in sulfur, and the tetrasulfide species is predominant (Table 1, first column). However, in the latter portions of the cell discharge, the trisulfide species is predominant. Near completion of the discharge, (Table 1, columns 2 to 4), the catholyte is nominally a K_2S_3, K_2S_2, and then a $K_2S_{1.2}$ solution.

Table 1. The distribution of polysulfide species in increasingly discharged cathodic solutions at 35°C. Calculated with the previously described computer iterative model (*20*) and equilibria constants (*18*). The final column is an expression of the alternative electrolyte in Fig. 2.

Species	Concentration (moles per liter)				
K_2S	4.5	4.5	4.5	4.5	4.5
Sulfur	13.5	9.0	4.5	1.0	4.5
KOH	0.0	0.0	0.0	0.0	3.38
$[S_2^{2-}]$	4×10^{-4}	0.07	0.2	0.1	0.7
$[S_3^{2-}]$	0.4	2.7	1.9	0.2	1.8
$[S_4^{2-}]$	3.7	1.2	0.2	0.003	0.06
$[S_5^{2-}]$	0.4	0.005	2×10^{-4}	4×10^{-7}	2×10^{-5}

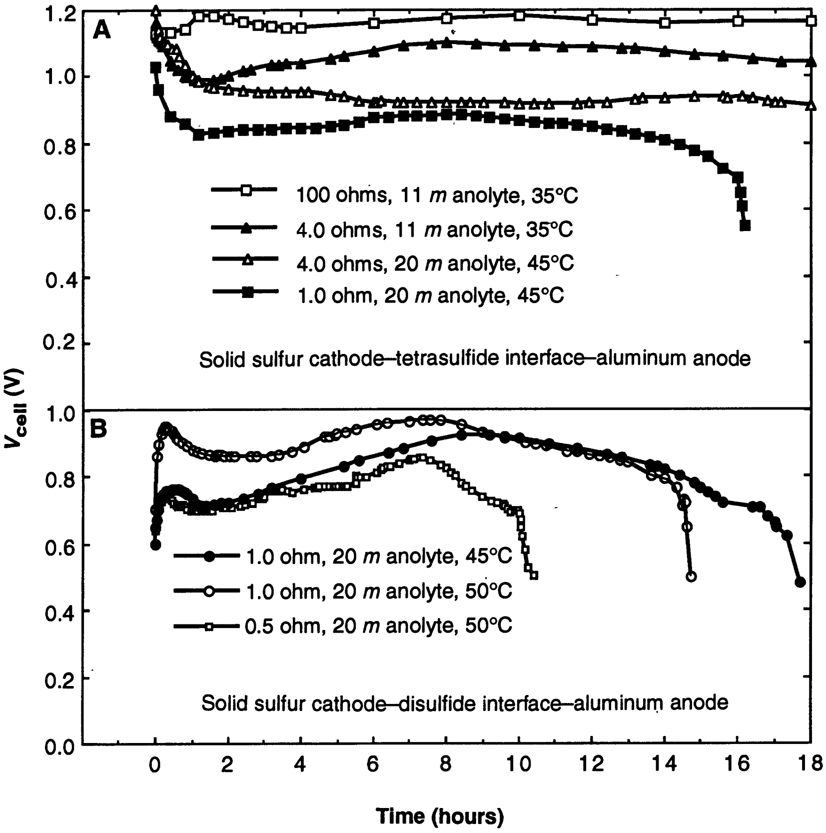

Fig. 3. Solid sulfur–aluminum discharge using a rectangular "D" cell configuration (*24*). The discharges were made through 1% precision resistors at the values indicated in ohms. The temperature was controlled with a thermostatic bath. In (**A**), the cathode contains 8.13 g of sulfur, the tetrasulfide interface consists of 0.006 liter of 7.7 *m* K_2S_4 catholyte without added KOH, and the anolyte is 0.040 liters of either 11 or 20.4 *m* KOH with 0.010 *m* $In(OH)_3$. In (**B**), the cathode utilizes a 0.006-liter interface of 6.5 *m* K_2S_2 catholyte and 4.9 *m* KOH.

Saturated sulfur-polysulfide solutions stored at room temperature for several months are stable (*21*). Furthermore, those solutions specifically measured for degradation at 45°C [with a previously described barium precipitation procedure (*22*)] show no measurable sulfur loss (to within the ±0.3% detection limits) over several days, although longer term testing is required. Giggenbach (*23*) has measured the reversible reaction of polysulfide solutions at elevated temperatures (over 150°C) and has shown that they spontaneously disproportionate to thiosulfate

$$S_5^{2-} + 3OH^- \rightarrow S_2O_3^{2-} + 3HS^- \tag{5}$$

This reaction will be parasitic to the solid sulfur cathode but is slow at moderate temperatures (*21*).

The solid sulfur cathode was incorporated into an aluminum cell analogous to the aluminum-polysulfide battery recently described (9). The discharge of aluminum in aqueous medium is accompanied by the formation of several aluminum species combined in the simplified anodic oxidation

$$Al + 3OH^- \rightarrow Al(OH)_3 + 3e^- \tag{6}$$

where $-E^\circ = -2.30$ versus SHE. From Eqs. 2 and 6, discharge of the aluminum–solid sulfur battery is expressed as

$$2Al + 3S + 3KOH + 3H_2O \rightarrow 2Al(OH)_3 + 3KHS \tag{7}$$

where $E_{cell} = 1.8$ V. Faradaic capacity of the Al-S battery (based on potassium salts) is 505 A·hour/kg, and the theoretical specific energy is 1.8 V × 505 A·hour/kg = 910 W·hour/kg, about 40% higher than that of the aluminum-polysulfide battery (9) and two to five times larger than that of conventional aqueous batteries. Utilization of lighter cations than K^+ may further improve the Al-S energy capacity.

In support of the proposed mechanism for discharge of the high-capacity solid sulfur cell given in Eqs. 2 through 4, Fig. 3 presents graphs of the discharge, at various rates, temperatures, and conditions, of a battery with a solid sulfur cathode, a polysulfide interface, and an aluminum anode. Typical open circuit voltages are 1.28 to 1.30 V. Under moderate to high rate conditions [1-ohm load over a "D" cell configuration (*24*)], the discharge time of 15 to 18 hours (Fig. 3) is over twice the 6.5-hour discharge obtainable in conventional alkaline batteries (*6*) and an increase of 30% compared with the previously described aluminum-polysulfide cell (*9*). The measured specific energy capacity of the Al-S battery (1-ohm discharge) is 220 W·hour/kg on the basis of active materials. Highly concentrated anolytes induce cathodic polarization losses (Fig. 3), a phenomenon that one can minimize by increasing cell temperature, increasing the ionic strength, or substituting disulfide for tetrasulfide in the catholyte interface.

The measured specific energy of 220 W·hour/kg of this cell can only provide an approximate comparison with the capacities of aqueous batteries in a more mature state of development. Conventional aqueous batteries typically achieve an experimental specific energy of 10 to 25% of the theoretical. The mechanically rechargeable Zn-air battery is considered to have a high measured specific energy of up to 110 W·hour/kg, and alkaline batteries with low discharge rates (Zn-MnO$_2$) have a specific energy of up to 95 W·hour/kg (*2*, *5*).

A further increase in Al-S power and specific energy may be accessible with a recently described Al-redox, mechanically rechargeable flow cell configuration with a high power density in which solvent may be recycled while electrolyte flows into and through the cell (*25*). The solid sulfur cathodes can support the requisite current densities for this configuration (Fig. 2, inset). This configuration, as modeled with an Al-ferricyanide battery, took advantage of the high currents sustainable for the reduction of ferricyanide (up to 0.5 A/cm^2 on planar electrocatalysts, and in excess of 2 A/cm^2 on porous electrocatalysts) and permitted better utilization of anode materials (*25*). Replacement of ferricyanide with a solid sulfur cathode may considerably enhance the energy capacity of this configuration.

REFERENCES AND NOTES

1. *Workshop on Advanced Battery Technology Research and Development*, Division of Chemical Sciences, Office of Basic Energy Science (U.S. Department of Energy, Washington, DC, 1992).
2. E. J. Cairns and F. R. McLarnon, in *Proceedings of the Symposium on Batteries and Fuel Cells for Stationary and Electric Vehicle Applications*, A. R. Landgrebe and A. Takehara, Eds. (Electrochemical Society, Pennington, NJ, 1993), vols. 93–98.
3. C. Scordilis-Kelley, J. Fuller, R. R. Carlin, J. S. Wilkes, *J. Electrochem. Soc.* **139**, 694 (1992).
4. N. Kuriyama, T. Sakai, H. Miyamua, I. Uehara, H. Ishikaras, *ibid.*, p. L72.
5. K. Y. Chu and R. F. Savinell, *ibid.* **138**, 1976 (1991).
6. D. Linden, *Handbook of Batteries* (McGraw-Hill, New York, 1984).
7. S. Licht, G. Hodes, R. Tenne, J. Manassen, *Nature* **326**, 863 (1987).
8. S. Licht, *J. Electrochem. Soc.* **134**, 2137 (1987).
9. ——— and D. Peramunage, *ibid.* **140**, L4 (1993).
10. From Eq. 2, 2 faradays of electrons are present for each mole of S and H_2O (0.032 + 0.018 kg). We can get the appropriate charge units per kilogram using standard conversions: 1 faraday = 96,500 C, 3600 C = 1 A·hour.
11. G. Hodes, J. Manassen, D. Cahen, *J. Electrochem. Soc.* **127**, 544 (1980).
12. P. Lessner, J. Winnick, F. R. McLarnon, E. J. Cairns, *ibid.* **133**, 2517 (1986).
13. S. Licht, *Nature* **330**, 148 (1987).
14. D. Lando, J. Manassen, G. Hodes, D. Cahen, *J. Am. Chem. Soc.* **101**, 3969 (1979).
15. N. Hartler, J. Libert, A. Teder, *Ind. Eng. Chem. Process Des. Dev.* **6**, 398 (1967).
16. ———, *Sven. Papperstidn.* **72**, 245 (1969); *Acta Chem. Scand.* **25**, 1722 (1971).
17. W. Giggenbach, *Inorg. Chem.* **11**, 1201 (1972).
18. ———, *ibid.* **13**, 1724 (1974).
19. S. Licht *et al.*, *J. Electroanal. Chem.* **318**, 111 (1991); S. Licht *et al.*, *Anal. Chem.* **62**, 1356 (1990); S. Licht *et al.*, *J. Electrochem. Soc.* **135**, 2971 (1988); S. Licht *et al.*, *ibid.* **134**, 918 (1987); S. Licht *et al.*, *ibid.* **133**, 277 (1986); S. Licht *et al.*, *ibid.* **132**, 1077 (1985).
20. S. Licht, G. Hodes, J. Manassen, *Inorg. Chem.* **25**, 2486 (1986).
21. S. Licht, J. Manassen, G. Hodes, *J. Electrochem. Soc.* **133**, 272 (1986).
22. S. Licht, *J. Phys. Chem.* **90**, 1096 (1986).
23. W. Giggenbach, *Inorg. Chem.* **13**, 1730 (1974).
24. The "D" cell configuration of 0.05 liter volume is described in (*9*) and contains a 60-cm^2 DH50V ALCAN aluminum anode in anolyte separated by a 60-cm^2 Raipore HD2291 membrane from solid sulfur in a catholyte polysulfide interface containing a 60-cm^2 thin-film CoS electrocatalytic cathode.
25. S. Licht and C. Marsh, *J. Electrochem. Soc.* **139**, L109 (1992).
26. A conventional three-electrode cell configuration and a Pine Instrument (Grove City, PA) RDE4 potentiostat-galvanostat were used to supply a constant current in the galvanostatic reduction of the cathodes. The cell contained cathode and counter (anode) compartments separated by a 3-cm^2 R1010 Raipore (Long Island, NY) cation-selective membrane. The cathode compartment consisted of solid (powdered) sulfur separated by a polypropylene mesh or polysulfide solution, or both. The 3-cm^2 CoS electrode (*9*) and a double-junction AgCl reference electrode were immersed in the polysulfide solution. The counter electrode compartment contained a DH50V ALCAN (Warren, NJ) aluminum electrode immersed in 13 m KOH, 0.010 m In(OH)$_3$, and 0.003 m Hg(NO$_3$)$_2$.

27. Supported in part by the National Science Foundation and the Clark University Carl Julius and Anna (Kranz) Carlson Chair in Chemistry.

16 April 1993; accepted 24 June 1993

Altered Growth and Cell Walls in a Fucose-Deficient Mutant of *Arabidopsis*

Wolf-Dieter Reiter,*† Clint C. S. Chapple,‡ Chris R. Somerville

A biochemical screening procedure was developed to identify mutants of *Arabidopsis thaliana* in which the polysaccharide composition of the cell wall was altered. Over 5000 ethyl methanesulfonate–mutagenized plants were analyzed by this method, leading to the identification of 38 mutant lines. One complementation group of mutants was completely deficient in L-fucose, a constituent of pectic and hemicellulosic polysaccharides. These mutant plants were dwarfed in growth habit, and their cell walls were considerably more fragile than normal.

The primary cell wall of higher plants determines cell shape and size during plant growth and development. Cell walls also provide mechanical support for plant tissues and organs and are intimately involved in a multitude of biological processes, such as cell-cell recognition and interaction, defense responses, and tropic responses (*1*). Plant cell walls are primarily composed of the polysaccharide components cellulose, hemicelluloses, and pectins (*2*). Cellulose microfibrils cross-linked by xyloglucan molecules are believed to serve as major load-bearing elements within the wall; however, the precise functions of the noncellulosic cell wall polysaccharides are poorly understood. To elucidate the roles of individual cell wall polysaccharides and to clone genes involved in their synthesis, we have taken a genetic approach by screening mutagenized *Arabidopsis* plants for alterations in their polysaccharide composition. One particularly informative class of mutant lines lacked fucose in their cell wall polysaccharides. Plants in this class had changes in their growth habit and in the mechanical properties of their walls.

From an ethyl methanesulfonate–mutagenized population of *Arabidopsis* plants (*3*), 5200 were screened for alterations in the monosaccharide composition of cell wall polysaccharides in leaves. For this purpose, acid hydrolysates of cell walls were analyzed by gas chromatography of alditol acetates (*4*). This screening strategy was based on the concept that many

---

Department of Energy Plant Research Laboratory, Michigan State University, East Lansing, MI 48824.

*To whom correspondence should be addressed.

†Address after 1 September 1993: Department of Molecular and Cell Biology, University of Connecticut, Storrs, CT 06269.

‡Address after 1 September 1993: Department of Biochemistry, Purdue University, West Lafayette, IN 47907.